PAPER • **OPEN ACCESS**

Efficient light harvesting in perovskite layer via three-dimensional TiO_2 nanobranched nanorod scaffold

To cite this article: Shervin Daneshvar e Asl *et al* 2020 *Nano Ex.* **1** 030017

View the article online for updates and enhancements.

The Electrochemical Society
Advancing solid state & electrochemical science & technology
2021 Virtual Education
Intensive Short Courses
Sun, Oct 10 & Mon, Oct 11
Providing students and professionals with in-depth education on a wide range of topics
Early registration deadline: Sep 13, 2021
Register early and save!



This content was downloaded from IP address 88.238.2.117 on 02/08/2021 at 00:20

NANO EXPRESS

PAPER

Efficient light harvesting in perovskite layer via three-dimensional TiO_2 nanobranched nanorod scaffold

Shervin Daneshvar e Asl[1], **Hamaneh Zarenezhad**[2,3], **Masoud Askari**[2], **Mohammad Halali**[2] and **Sayed Khatiboleslam Sadrnezhaad**[1,2]

[1] Advanced Bionanomaterials Laboratory, Department of Materials Science and Engineering, Sharif University of Technology, Tehran, Iran
[2] Department of Materials Science and Engineering, Sharif University of Technology, Tehran, Iran
[3] Koç University, TÜPRAŞ Energy Center (KUTEM), Istanbul, Turkey

E-mail: sh_daneshvarasl@alum.sharif.edu **and** sh_daneshvarasl@yahoo.com

Keywords: Titanium dioxide, Three-dimensional scaffold, Nanobranched nanorod, Thin film, Solar cell

OPEN ACCESS

RECEIVED
12 August 2020

REVISED
22 October 2020

ACCEPTED FOR PUBLICATION
28 October 2020

PUBLISHED
5 November 2020

Original content from this work may be used under the terms of the Creative Commons Attribution 4.0 licence.

Any further distribution of this work must maintain attribution to the author(s) and the title of the work, journal citation and DOI.

Abstract

A comparative study was done on three types of TiO_2 thin film morphology, i.e., mesoporous nanoparticles, nanorods, and nanobranched nanorods thin films, as the scaffold for the perovskite solar cell. The performances of the perovskite-coated thin films were compared in terms of charge carrier extraction, charge transport, and solar energy harvesting via photoluminescence and UV–vis spectroscopies. TiO_2 nanobranched nanorods thin film showed better photovoltaic performance than those of mesoporous nanoparticles and nanorods thin films. The better optical properties of nanobranched nanorods thin film as the scaffold is ascribed to its unique morphological advantages, i.e., remarkable specific surface area along with high-speed pathways for charge carriers. These characteristics lead to great, compact, and uniform perovskite loading, excellent electron transport property, and desired light harvesting performance, which are preferable features for promoting the efficiency of the perovskite solar cells. This paper introduces an outstanding scaffold for fabrication of high-performance perovskite solar cells.

1. Introduction

High photovoltaic efficiency, low production cost, and easy fabrication by solution processes make inorganic halide perovskite solar cells (PSCs) the most promising candidate among various types of solar cells [1–8]. A typical PSC with a p-i-n junction configuration includes five layers. A light absorbent perovskite layer places between an n-type electron transfer layer (ETL) and a hole transport layer (HTL). ETL and HTL layers are generally TiO_2 and p-type organic semiconductor (spiro-OMeTAD), respectively. At i–n and p–i interfaces, the separation of the photogenerated charges occurs through *in situ* electrical field. Photogenerated electrons and holes collect by the FTO and cathode (e.g., Ag) layers, respectively [9–13]. Inadequate light absorption, short diffusion lengths of charge carriers, and charge recombination are the most significant reasons for limited power conversion efficiency of solar cells [14]. High specific surface area and fast charge transport are preferable features for solar cells [15].

Mesoporous nanoparticles based scaffold provides large surface area but suffers from poor electron mobility. On the other hand, one-dimensional nanomaterials such as nanorods and nanowires represent rapid electron conducting. However, their low surface area compensates their favorable advantage. Due to their remarkable specific surface area along with high-speed pathways for charge carriers, three-dimensional (3D) hierarchical nanostructures are outstanding candidates for photoelectrochemical application [16–19]. Daneshvar e Asl and Sadrnezhaad [20] successfully synthesized TiO_2 nanoleafed nanorods thin film, and evaluated it as a novel-designed photocatalyst for the photodegradation of anionic and cationic dyes. The improved photocatalytic performance of TiO_2 is ascribed to large surface area and desirable light harvesting. Chen *et al* [21] reported a novel facile and one-step synthesis of hierarchical TiO_2 nanotubes, and used this

© 2020 The Author(s). Published by IOP Publishing Ltd

nanostructure in fabrication of the photoelectrode of the dye-sensitized solar cell. Considerable obtained efficiency of 9.89% is attributed to directed charge transport, excellent light harvesting, and effective charge collection. Li *et al* [22] successfully prepared stainless steel mesh-supported 3D hierarchical SnO_2/Zn_2SnO_4 composite for gas sensor, solar cell, and photocatalysis applications. Xu *et al* [23] synthesized sheet-like CdS sensitized ZnO film by hydrothermal method. The photoelectrochemical property enhancement is ascribed to the improved light absorption and enhanced charge separation and transportation.

In this paper, TiO_2 mesoporous nanoparticles, nanorods, and nanobranched nanorods thin films were synthesized and utilized as the scaffold for perovskite coating for further use in PSCs. The performance of the thin films were compared in terms of charge carrier extraction, charge transport, and solar energy harvesting through photoluminescence and UV–vis spectroscopies. Perovskite-coated TiO_2 nanobranched nanorods thin film showed the best photovoltaic performance due to desirable characteristics of nanobranched nanorods thin film.

2. Experimental

2.1. Materials

Analytical-grade raw materials were bought from the following producers:

(a) Fluorine-doped tin oxide (FTO) glass and TiO_2 paste (18 NR-T) from Dyesol Company,

(b) Titanium butoxide, titanium tetrachloride, acetone, ethanol, 2-propanol, hydrochloric acid, and sodium chloride from Merck, and

(c) Titanium isopropoxide (TTIP), ammonium hexafluo-rotitanate, lead iodide, N,N-dimethylformamide (DMF), methylammonium iodide (MAI) powder, zinc powder, boric acid, and iso-propanol from Sigma-Aldrich.

2.2. Synthesis

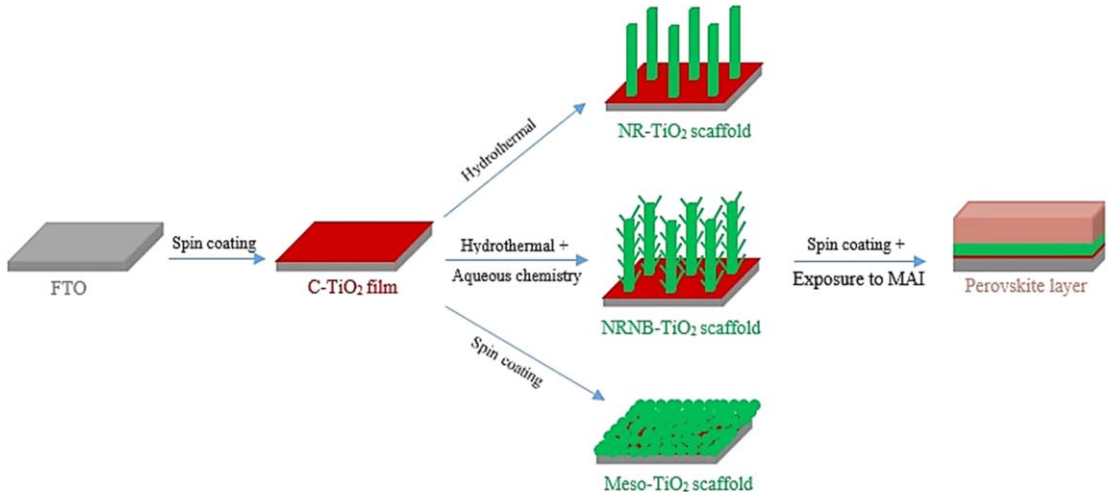
A patterned FTO substrate was prepared via chemical etching with hydrochloric acid and zinc powder. TTIP was mixed with ethanol to make the solution precursor of compact TiO_2 (C-TiO_2) film. C-TiO_2 film were coated on the patterned FTO by spin coating under 2000 rpm for 60 s followed by heating at 80 °C and 500 °C for 10 min and 30 min, respectively. Then, three types of TiO_2 scaffold were deposited on the C-TiO_2 film. Mesoporous nanoparticles (Meso) film was prepared by spin coating TiO_2 paste diluted in ethanol with weight ratio of 1:7 under 4000 rpm for 30 s. Nanorods (NR) and nanobranched nanorods (NRNB) thin films were synthesized on top of C-TiO_2 film via the hydrothermal and aqueous chemistry methods according to our previous work [24]. The coated TiO_2 thin films were annealed at 450 °C for 30 min. For perovskite layer coating, a solution of lead iodide in DMF (1 M) with 70 °C temperature was spin coated on the TiO_2 scaffold at 6500 rpm for 5 s, and dried at 100 °C for 30 min. Then, the layers were exposed to MAI powder in the oven with 150 °C temperature for 2 h. After cooling in ambient temperature, the layers were cleaned by iso-propanol, and then heated at 140 °C for 30 min. The synthesis procedure are summarized in Scheme 1.

2.3. Instrumentations and characterizations

Morphological surface and cross-sectional images of bare and perovskite-coated TiO_2 thin films were taken on a field emission scanning electron microscope (FESEM; MIRA3TESCAN-XMU). The composition and crystal structure of the layers were evaluated by the x-ray diffractometer (XRD) (X′Pert PRO MPD (PANalytical) with Cu Kα radiation). The light absorption characteristics of the perovskite layers on various TiO_2 scaffolds were investigated by UV–Vis spectrophotometer (Avaspec-2048-TECwith AvaLamp DH-S Setup) with an integrating sphere attachment. Steady-state and time-resolved photoluminescence (Pl) of the perovskite layers were measured by Avaspec 2048 TEC spectrophotometer.

3. Results and discussion

FESEM analysis was employed to study the effect of TiO_2 scaffold morphology on the quality of upper perovskite layer. It was thus possible to understand the correlation between crystal growth behavior and grain size with perovskite layer quality. FESEM images of three types of TiO_2 thin film, i.e., Meso, NR, and NRNB, as well as perovskite layer coated on them are shown in figure 1. As it is clear in figures 1(a)–(c), TiO_2 thin films are crack-free and monotonously covered the substrate surface. The trunk of NRNB structure could provide a fast charge pathway to improve electron collection and probably decrease hysteresis effect compared with Meso structure. In analogy with NR arrays, the 3D morphology of NRNB make much higher volume density available for the



Scheme 1. Preparation procedure of perovskite layer onto different TiO_2 scaffolds.

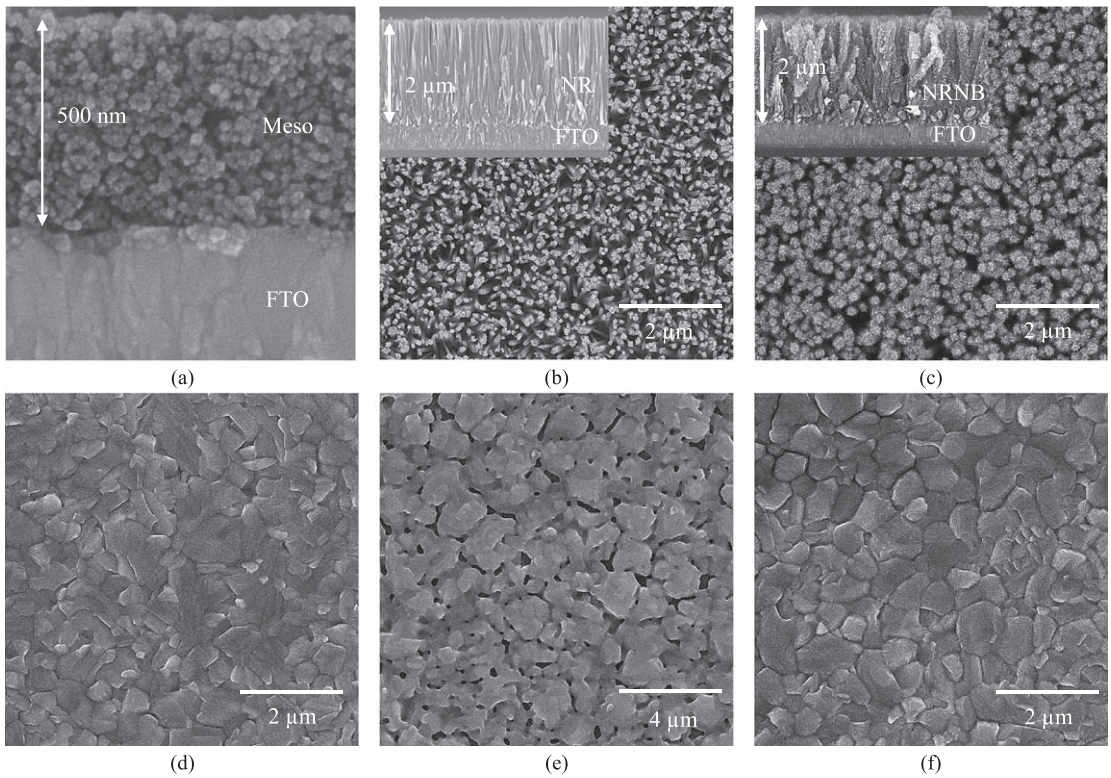


Figure 1. FESEM images of TiO_2 (a) Meso, (b) NR, and (c) NRNB thin film and of perovskite layer coated on TiO_2 (d) Meso, (e) NR, and (f) NRNB. The insets of (b) and (c) show images of the cross-sectional view of TiO_2 NR and NRNB thin films.

nucleation of perovskite layer. Moreover, this structure could increment the optical pathways through light scattering. Also, NBs present in the space between NRs could extract photogenerated electrons from $MAPbI_3$ to overcome the hindrance of short electron diffusion length in the $MAPbI_3$. Figures 1(d)–(f) shows surface images of perovskite layers prepared onto different TiO_2 scaffolds. Perovskite layer formed on TiO_2 NRNB is more compact and has fewer voids than those obtained by TiO_2 Meso and NR scaffolds. This observation may be attributed to the slower rate of inter diffusion and reaction between the MAI vapor and the PbI_2 film in presence of TiO_2 NRNB. In both TiO_2 NRNB and Meso, nucleation and growth of perovskite is greatly affected by the scaffold. The coating behavior of the perovskite layer is improved by using TiO_2 NRNB. A perovskite capping layer with high coverage helps enhance light absorption and improve the performance of the solar cell. A large proportion of voids can be seen in perovskite layer that was processed by TiO_2 NR. In this sample, there is a high

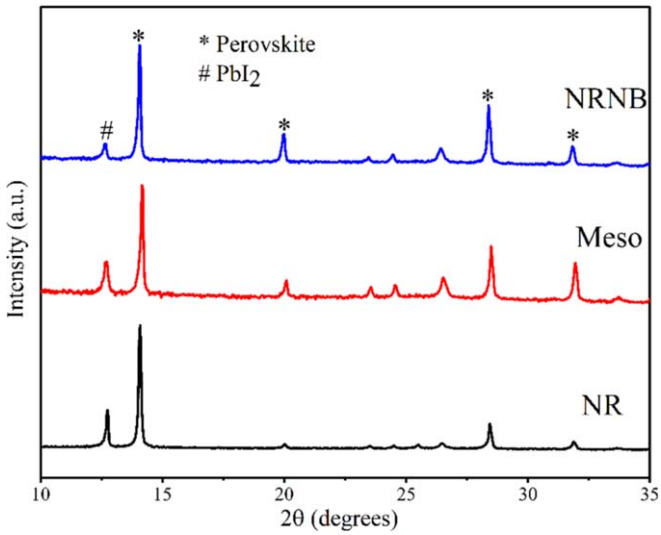


Figure 2. XRD patterns of perovskite layers coated on various TiO_2 thin films.

probability of contact between the ETL and HTL. As a result, charge carrier species, i.e., electrons and holes, may recombine within the perovskite layer, and it decreases efficiency of the solar cell.

For a complete study of the nature of perovskite layers coated on different TiO_2 scaffolds, XRD analysis was employed (figure 2). Similarity in the XRD patterns between perovskite samples prepared on various TiO_2 scaffolds indicates that all scaffolds produce the same perovskite. The 2θ values of 31.8°, 28.4°, and 14.1° are the main peaks for perovskite crystals. These values correspond to (310), (220), and (110) lattice planes of tetragonal perovskite crystalline structure, respectively [25–28]. Also, as pointed out in figure 2, a peak is observed at 12.7°, corresponding to the (001) lattice plane. This peak relates to the not-reacted PbI_2. In other words, the conversion to perovskite is incomplete. The strongest peak for residual PbI_2 is observed in perovskite layer with NR scaffold. The sample prepared in the presence of NRNB scaffold exhibits the weakest peak of PbI_2, indicating a near complete transformation to perovskite. A large fraction of residual PbI_2 in perovskite layer is expected to be harmful to the solar cell efficiency. This is mainly results from the electrical insulating nature of PbI_2 [29, 30].

To determine the optical properties of perovskite layers deposited on various TiO_2 thin films, UV–vis absorption spectra were acquired. The absorption range from 400 nm up to 750 nm is shown for all prepared layers in figure 3, which indicates the formation of perovskite on the TiO_2 scaffolds. The UV–vis absorption is initially improved in presence of TiO_2 NRNB scaffold. Generally, full coverage and compact perovskite layer can increase the UV–vis absorption [31, 32], which can approve the highest UV–vis absorption for perovskite layer deposited on top of TiO_2 NRNB scaffold. A decline in the light absorption is seen for the TiO_2 NR-based perovskite layer, which derives from the partially coverage of perovskite layer with higher voids.

To comprehensive study of the optical properties of perovskite layers, Pl spectrums of the perovskite-TiO_2 films were measured. In general, the charge carrier extraction in the perovskite layer is mainly dependent on the perovskite layer morphology. Figure 4(a) displays the steady-state Pl spectrums of perovskite layers deposited on different TiO_2 films. The Pl intensity decrease indicates effective charge carrier extraction happens within the perovskite-TiO_2 films [33–35]. The higher Pl intensity of perovskite-TiO_2 NR is resulted from an inhomogeneous perovskite layer with a high number of voids. A low Pl intensity can be seen for perovskite-TiO_2 NRNB, that is attributed to high coverage and compactness of perovskite layer. Thus, the steady-state Pl analysis indicates that the high charge carrier extraction efficiency occurs in the uniform and smooth perovskite layer. To study the charge carrier extraction/transfer behavior, the time-resolved Pl decay spectra of different perovskite-TiO_2 films were measured, as presented in figure 4(b). The shortest Pl decay lifetime can be seen for the perovskite-TiO_2 NRNB scaffold, which shows the faster charge carrier transfer into ETL and HTL. An efficient and fast charge carrier extraction and transfer process into charge carrier layers results from the compact and unharmed perovskite layer-TiO_2 scaffold interface. An inhomogeneous and partially coverage perovskite layer with voids can provide recombination sites, which leads to an insufficient charge carrier extraction/transfer. The Pl decay lifetimes for the perovskite layers prepared onto different TiO_2 scaffolds were 14.11, 17.21 and 19.99 for TiO_2-NRNB, TiO_2-Meso, and TiO_2-NR, respectively. It is well-known that the charge carriers generated in the perovskite domain can be injected into ETL, and the PL of perovskite layers occurs due to the recombination of localized charge carriers. The spectrum of perovskite layer prepared with TiO_2-NRNB substrate shows a significant depressed PL (14.11 ns) compared with that of the layers with TiO_2-Meso and

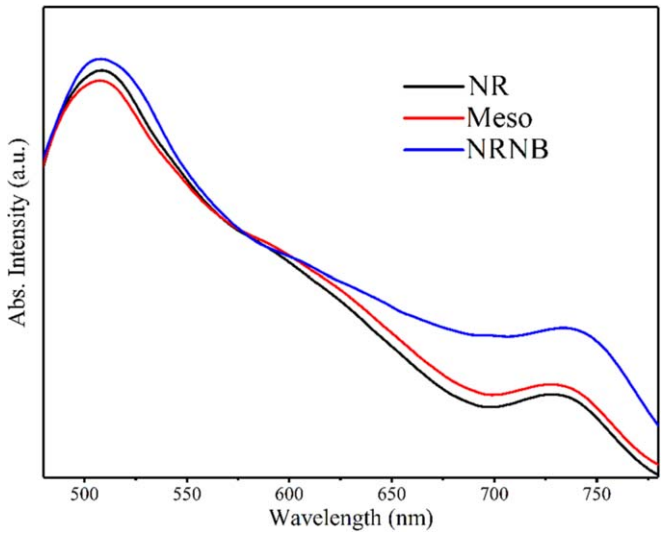


Figure 3. UV–Vis absorption spectra of perovskite layers coated on different TiO_2 thin films.

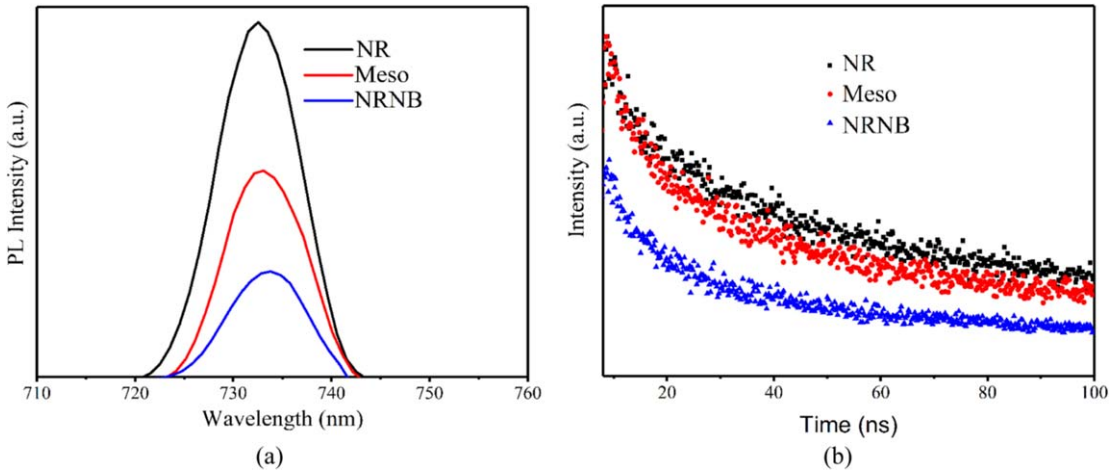


Figure 4. (a) Steady-state and (b) time-resolved Pl spectrums of perovskite layers coated on different TiO_2 thin films.

TiO_2-NR (17.21 ns and 19.99 ns, respectively), indicating that the charge carriers generated can be effectively generated and extracted. In fact, the diffusion length of charge carriers is increased by 21% and 40% in presence of TiO_2-NRNB substrate compare with TiO_2-Meso and TiO_2-NR, respectively.

4. Conclusions

Three types of TiO_2 thin film, i.e., mesoporous nanoparticles, nanorods, and nanobranched nanorods, were synthesized and used as the scaffold for perovskite coating for further use in the perovskite solar cell. Hierarchical nanobranched nanorods thin film presented better optical properties compared with thin films of mesoporous nanoparticles and nanorod arrays. In fact, the large surface area and charge transport property of nanobranched nanorods led to uniform and compact perovskite loading, excellent electron collection, and desired light harvesting performance, which are preferable features for promoting the efficiency of the perovskite solar cells.

Acknowledgments

This work was partially supported by the Iran National Science Foundation.

Conflicts of interest or competing interests

The authors declare that they have no known competing financial interests or personal relationships that could have appeared to influence the work reported in this paper.

Data availability

The data that support the findings of this study are available upon request from the authors.

ORCID iDs

Shervin Daneshvar e Asl https://orcid.org/0000-0002-4643-3747
Sayed Khatiboleslam Sadrnezhaad https://orcid.org/0000-0003-2631-5863

References

[1] Luo Y *et al* 2016 Fine control of perovskite-layered morphology and composition via sequential deposition crystallization process towards improved perovskite solar cells *J. Power Sources* **311** 130–6
[2] Wang M *et al* 2018 Performance improvement of perovskite solar cells through enhanced hole extraction: The role of iodide concentration gradient *Sol. Energy Mater. Sol. Cells* **185** 117–23
[3] Li Y, Guo Y, Li Y and Zhou X 2016 Fabrication of Cd-doped TiO_2 nanorod arrays and photovoltaic property in perovskite solar cell *Electrochim. Acta* **200** 29–36
[4] Kazim S, Nazeeruddin M K, Grätzel M and Ahmad S 2014 Perovskite as light harvester: a game changer in photovoltaics *Angew Chemie Int Ed* **53** 2812–24
[5] Gao P, Grätzel M and Nazeeruddin M K 2014 Organohalide lead perovskites for photovoltaic applications *Energy Environ Sci Sci* **7** 2448–63
[6] Jung H S and Park N-G 2014 Perovskite solar cells: from materials to devices *Small* **11** 1–16
[7] Green M A, Ho-baillie A and Snaith H J 2014 The emergence of perovskite solar cells *Nat. Photonics* **8** 506–5014
[8] Stranks S D and Snaith H J 2015 Metal-halide perovskites for photovoltaic and light-emitting devices *Nat. Nanotechnol.* **10** 391–402
[9] Zarenezhad H *et al* 2020 Enhanced electron transport induced by a ferroelectric field in efficient halide perovskite solar cells *Sol. Energy Mater. Sol. Cells* **206** 110318
[10] Yang X *et al* 2018 Progress in hole-transporting materials for perovskite solar cells *J Energy Chem* **27** 650–72
[11] Zhen C *et al* 2019 Strategies for modifying TiO_2 based electron transport layers to boost perovskite solar cells. *ACS Sustain Chem Eng* **7** 4586–618
[12] Yang S *et al* 2019 Highly efficient and stable planar $CsPbI_2Br$ perovskite solar cell with a new sensitive-dopant-free hole transport layer obtained via an effective surface passivation *Sol. Energy Mater. Sol. Cells* **201** 110052
[13] Wang Z *et al* 2019 Solution processed Nb_2O_5 electrodes for high efficient ultraviolet light stable planar perovskite solar cells. *ACS Sustain Chem Eng* **7** 7421–9
[14] Schulz P, Cahen D and Kahn A 2019 Halide perovskites: is it all about the interfaces? *Chem. Rev.* **119** 3349–417
[15] Grätzel M 2001 Photoelectrochemical cells *Nature* **414** 338–44
[16] Cheng C and Fan H J 2012 Branched nanowires: synthesis and energy applications *Nano Today* **7** 327–43
[17] Cho I S *et al* 2011 Branched TiO_2 nanorods for photoelectrochemical hydrogen production *Nano Lett.* **11** 4978–84
[18] Wang X, Li Z, Shi J and Yu Y 2014 One-dimensional titanium dioxide nanomaterials: Nanowires, nanorods, and nanobelts *Chem. Rev.* **114** 9346–84
[19] Daneshvar e Asl S and Sadrnezhaad S K 2020 Biphasic TiO_2 nanoleafed nanorod electrode for dye-sensitized solar cell *Phys E Low-dimensional Syst Nanostructures* **123** 114206
[20] Daneshvar e Asl S and Sadrnezhaad S K 2020 Anionic and cationic pollutants degradation via TiO_2 nanoleafed nanorods *Solid State Sci.* **105** 106263
[21] Chen H *et al* 2020 A novel cheap, one-step and facile synthesis of hierarchical TiO_2 nanotubes as fast electron transport channels for highly efficient dye-sensitized solar cells *Adv. Powder Technol* **31** 1556–63
[22] Li Z *et al* 2020 Stainless steel mesh-supported three-dimensional hierarchical SnO_2/Zn_2SnO_4 composite for the applications in solar cell, gas sensor, and photocatalysis *Appl. Surf. Sci.* **502** 144113
[23] Xu S *et al* 2020 Construction of ZnO/CdS three-dimensional hierarchical photoelectrode for improved photoelectrochemical performance *Renew Energy* **153** 241–8
[24] Daneshvar e Asl S, Eslami Saed A and Sadrnezhaad S K 2019 Hierarchical rutile/anatase TiO_2 nanorod/nanoflower thin film: synthesis and characterizations *Mater. Sci. Semicond. Process.* **93** 252–9
[25] Chen Q *et al* 2014 Planar heterojunction perovskite solar cells via vapor-assisted solution process *J. Am. Chem. Soc.* **136** 622–5
[26] Im J-H *et al* 2011 6.5% efficient perovskite quantum-dot-sensitized solar cell *Nanoscale* **2** 4088–93
[27] Qaid S M H *et al* 2016 Band-gap tuning of lead halide perovskite using a single step spin-coating deposition process *Mater. Lett.* **164** 498–501
[28] Kumar Y *et al* 2016 Effect of heat treatment on the electrical properties of perovskite solar cells *Sol. Energy Mater. Sol. Cells* **157** 10–7
[29] Murugadoss G *et al* 2016 An efficient electron transport material of tin oxide for planar structure perovskite solar cells *J. Power Sources* **307** 891–7
[30] Supasai T *et al* 2013 Formation of a passivating $CH_3NH_3PbI_3/PbI_2$ interface during moderate *Appl. Phys. Lett.* **103** 183906
[31] Ding Y *et al* 2014 Surfactant enhanced surface coverage of $CH_3NH_3PbI_{3-x}Cl_x$ perovskite for highly efficient mesoscopic solar cells *J. Power Sources* **272** 351–5
[32] Song X *et al* 2015 Additive to regulate the perovskite crystal film growth in planar heterojunction solar cells *Appl. Phys. Lett.* **106** 033901

[33] Zeng X *et al* 2017 Performance improvement of perovskite solar cells by employing a CdSe quantum dot/PCBM composite as an electron transport layer *J Mater Chem A* **5** 17499–505
[34] Sun C *et al* 2016 Enhanced photovoltaic performance of perovskite solar cells using polymer P(VDF-TrFE) as a processed additive *J. Phys. Chem. C* **120** 12980–8
[35] Zheng H *et al* 2019 The multiple effects of polyaniline additive to improve the efficiency and stability of perovskite solar cells *J Mater Chem C* **7** 4441–8